Available online at www.sciencedirect.com

ScienceDirect

Procedia Computer Science 218 (2023) 542–553

Procedia Computer Science

www.elsevier.com/locate/procedia

International Conference on Machine Learning and Data Engineering

3D MRI Segmentation using U-Net Architecture for the detection of Brain Tumor

Smarta Sangui[a], Tamim Iqbal[a], Piyush Chandra Chandra[a], Swarup Kr Ghosh[a], Anupam Ghosh[b]*

a Sister Nivedita University, Kolkata 700156, India
b Netaji Shubash Engineering College, Kolkata 700152, India

Abstract

Segmentation of brain tumor from 3D images is one of the most important and difficult tasks in the field of medical image processing as a manual human-assisted categorization can result in incorrect prediction and diagnosis. Furthermore, it is a difficult process when there is a huge amount of data to assist. Extracting brain tumour regions from MRI images becomes challenging due to the great variety of appearances of brain tumours and how similar they are to normal tissues. In this paper, we have designed modified U-Net architecture under a deep-learning framework for the detection and segmentation of brain tumors from MRI images. The applied model has been evaluated on genuine images provided by Medical Image Computing and Computer-Assisted Interventions BRATS 2020 datasets. Test accuracy of 99.4% has been achieved using the above-mentioned dataset. A comparative review with other papers shows our model using U-Net performs better than other deep learning-based models.

Keywords: BRATS, brain tumor, segmentation, MRI, U-net, tumor detection.

1. Introduction

Medical image processing is a technique and method for generating a visual depiction of the body's inside, as well as a function of some organ or tissue, for clinical research and medical treatment [31]. Medical images are designed to highlight concealed internal structures for illness detection and treatment. Medical imaging also generates a database of regular anatomical structures and physiology to aid in the detection of anomalies [22].

Medical image processing refers to the manipulation of images using a computer. This process involves various types of techniques and operations, such as retrieving, saving, displaying, and communicating images [33]. This process follows the detection and handling of incidents and a database of the normal structures and functions of an organ, making it easier to identify abnormalities. It includes both organic and radiographic imaging using electromagnetic energy (X-Ray and gamma rays), ultrasonography [34], magnetism, oscilloscope, thermal, and isotope imaging. There are many other strategies for recording data regarding body position and function. These techniques have many limitations compared to the modular that produces the image [32].

One of the image processing techniques is to use a computer for the alteration of digital images. This technique has many advantages such as restoring force, adaptability, data storage, and communication. As various image resizing

1877-0509
10.1016/j.procs.2023.01.036

technologies grow, you can save images efficiently. This technique has many rulesets for running images synchronously [35].

There might be different kinds of anomalies in the brain, but the most likely among them are brain tumors. Brain tumors occur due to abnormal cell growth in the brain. The brain's structure is extremely complicated, where several regions are in charge of various nervous system activities [23]. Tumors can form anywhere in the brain or skull, including the protective linings, the base of the brain, and other regions. There are different kinds of brain tumors that exist and they depend on what tissue they arise from [27][29].

Each year, tens of thousands of individuals are diagnosed with brain tumors. [2], deep learning algorithms have sparked interest in the automated diagnosis and categorization of brain tumors. These techniques have also been used in the segmentation of brain tumors, and the medical world is paying close attention to this field [3]. The purpose of segmentation is to change how various portions of an image are represented, making it easier to interpret areas of the image with distinct properties. Each area becomes spatially contiguous after separating the picture of the brain into these many distinct sections [4][22]. The lengthy-time requirements and the possibility of misclassification due to the problem's complexity are two prominent challenges in the manual identification of brain tumors. As a result, automated segmentation of the brain MRI images can greatly enhance diagnosis and treatment procedures, particularly when access to radiologists and qualified experts is limited [24] [30].

Many research studies can be found related to x-ray or CT images but works on MRI image segmentation are comparatively less. MRI images are hard to handle due to a large hardware dependency and they also have an extra one or more extra dimensions which is different from typical RGB images. Each image can very well be bigger than 1GB. The computation and space required for training large MRI datasets are very high.

Every year, thousands of people are diagnosed with brain tumors globally. This has sparked interest in the field of automated diagnosis and categorization of brain tumors using deep learning algorithms. The main purpose of segmentation is to change how segments of a picture are represented making it easier to interpret regions of images with distinct properties. Each area becomes spatially contiguous after separating the picture of the brain into distinct sections. This lengthy time requirement and the possibility of misclassification due to the problem of complexity are two prominent challenges in the identification of manual detection of brain tumors. Hence, automatic segmentation of 3D MRI images of the brain can greatly improve diagnosis and treatment procedures, especially when access to qualified medical experts and radiologists is limited. Inspired by UNet which is designed for handling medical images we have used it here for brain tumor segmentation using 3D MRI images.

1.1 Motivation

MRI is the most sensitive imaging test for investigating the brain and spinal cord anatomy. It works by stimulating hydrogen protons in the tissue, which sends an electromagnetic signal return to the MRI machine. The MRI machine senses the intensity and transforms it into a grayscale MRI scan.

Therefore, the terms high and low signal are used to describe the MRI appearance of the part of the brain with the gray matter as the reference point. This means that anything brighter than gray matter has a high signal and darker ones have a low signal. For example, in all sequences, bone has the lowest proton density, resulting in the darkest structure in the scan. It is worth mentioning that MRI may be used in combination with contrast media such as gadolinium. Radiological contrast increases the visual contrast between the inspected structure and the tissue that surrounds it.

1.2 Contribution

In order to accomplish brain tumor segmentation and classification, deep learning is going to be used here. The 3D MRI images are taken in ".nii" format. We have modified the basic U-Net architecture for 3D image segmentation for brain tumor detection from brain MRI. The modified U-Net architecture is used in which Images will be downsampled to a very low resolution for feature extraction and after classifying the image will be upsampled to the original size. The designed architecture in deep learning framework has been utilized to train the model from BRATS 2020 dataset for the prediction. The suggested model has predicted four types of tumors in the brain which have been validated with ground truth. This saved model will help us to classify and identify the presence of any tumor in the brain.

2. Literature Review

The authors in [5] have discussed a binary classification problem with MRI images of brain tumors. For feature extraction, they used ALEXnet and VGG16 and a recurrent feature elimination (RFE) is performed. Finally, for the classification task, they used a Support Vector Machine (SVM), which provided an overall accuracy of 96%. For tumor detection and segmentation, Sakshi et al. [1] employed transfer learning followed by superpixel techniques. The tumor was split into two groups using the superpixel approach. In contrast to ground truth data, this delivered 0.93 of the average dice index.

To obtain reliable MRI scan findings, Choudhury et al. [6] and Ghosh et al. [20] utilised deep learning approaches incorporating deep neural networks and combined them with a CNN model. A three-layered CNN architecture was presented, including a fully linked neural network as a backbone. The F-score was 97.33%, while the accuracy was 96.05%. Rehman et al. [42] proposed a 3D CNN (pre-trained VGG19) architecture for tumor extraction and transfer learning was used for classification which gave an accuracy of 98.32 on the BRATS 2015 dataset. Tripathi et al. [2] proposed a technique where the segmentation tasks are performed utilizing an OKM technique. Otsu thresholding and K-Means clustering, two widely used ideas, are the core components of the OKM method. Results showed a dice coefficient greater than 0.70 for all the cases.

Ahmad Habbie et al. [7] examined the possibility of a tumor in the brain on MRI T1 weighted images using semi-automated segmentation utilizing an active contour model. According to the data, MGAC performed the best of the three. In [8], the authors describe a modified and enhanced form of the RESnet50 that performed better in the classification of brain MRI images into two categories, tumor and non-tumor. The results are compared to well-known CNN designs like Googlenet, Alexnet, and DENSEnet, among others. The suggested approach provides an accuracy of 97 %. The authors of [9] took advantage of classification accuracy and error rate's impact on data preprocessing. After that, to reduce overfitting, the dataset was extended using seven augmentation approaches. Finally, the enlarged dataset of MRI scans is fed into the Resnet50 architecture, which is utilized for training and testing. The accuracy of the results is 98 % [15].

Özyurt et al. [14] presented a hybrid technique known as SR-FCM-CNN. They used the SR CNN network to accomplish the pre-processing. This method converts low-resolution photos to high-resolution images, which are subsequently segmented with the FCM method. The Squeeze-net architecture was then used to extract features, which were then categorized using the ELM method. The accuracy rating is 98 %. For the classification of three different categories of brain tumors, Badža et al. [10] formulated a new kind of CNN architecture. And to evaluate the network's performance four techniques were used: a unique combination of two 10-fold cross-validation methodologies and two databases. One of the 10-fold procedures, subject-wise cross-validation, was used to evaluate the network's generalisation capacity. And an improved image database was used to test the progress. The 10-fold cross-validation procedure's best result was obtained using record-wise cross-validation for the enhanced data set, which had an accuracy of 96.56%. For brain tumor classifications utilizing capsule networks, Parnian Afshar et al. [11] employed a Bayesian technique. A capsule network was utilized instead of CNN to improve tumor identification outcomes because a CNN may lose essential spatial information. Teshnehlab. et al. [12] utilized a Convolutional Neural Network (CNN) for detecting a tumor. The classification accuracy of the Fully Connected Softmax plate, which was used to categorize images, was 98.67 %. With the Radial Basis Function (RBF) classifier, the CNN's precision is also 97.34 %, and with the Decision Tree (DT) classifier, it's 94.24 % [16][17].

3. Methodology

The main research methodology that has been used is classification research in which the brain tumor is going to be classification and comparative research where the obtained classification will be compared with other classifications in order to study the improvements obtained. In order to train the model, 3D MRI images have been needed. The data for this paper was collected from the BRATS2020 dataset which was available publicly. The dataset was already grouped into images for training and testing. Then the tumor regions were defined in the high-resolution 3D MRI images by using U-Net Model to downsample the images into a lower resolution in order to identify the features more efficiently, this part is also known as the encoder path. And then again the images are upsampled with the preserved extracted feature also known as the decoder path. This is used to locate and differentiate boundaries by performing classification on each pixel, resulting in the input and output having the same size [36]. So in the downsampling or

encoder path, our model gets to know “WHAT” is present in the image and in the upsampling or decoder path the model recovers the “WHERE” information (or where is it present in the image).

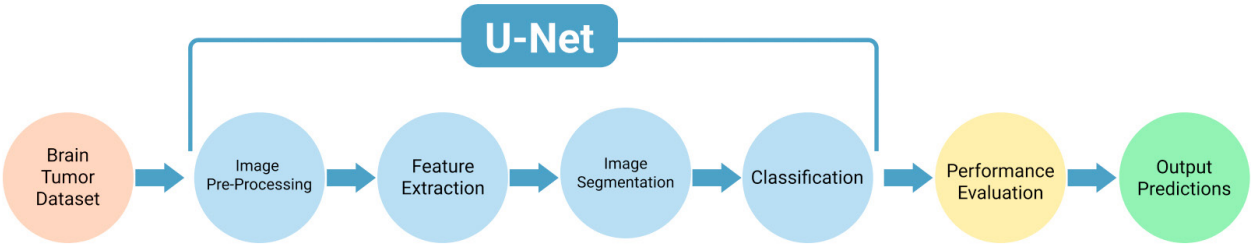

Figure 1: Block Diagram of proposed methodology

After collecting the BRATS dataset the images were pre-processed and then segmentation was performed according to various classes like no tumor, edema, necrotic/core, and enhancing tumor. Further during training feature extraction was done concerning the tumor and classified accordingly. Finally, the model predicted the output based on the results and it was stored for future evaluation and performing a comparative analysis. The Process flow diagram in Fig. 2 shows the journey of the implementation of the paper from beginning to end.

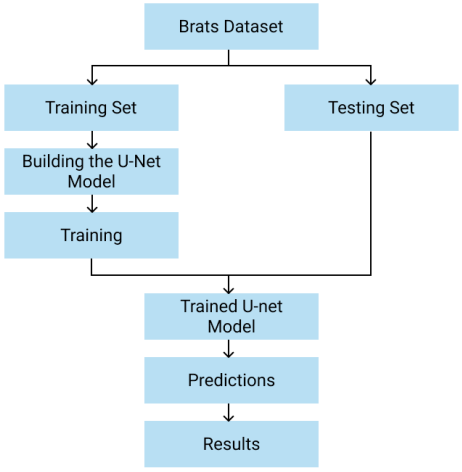

Figure 2: Implementation process

3.1 Exploring and Visualizing the dataset:

The image dataset used in the paper is the Brats2020 dataset which contains 3D MRI in “nii” format. In order to properly visualize the dataset and understand the images to perform further operations, several neural imaging libraries such as “nilearn” and “nibabel” were used. These libraries were used to load the “nii” images and plot the images in different forms. Given below is a visual representation of an MRI image. Figure 3 shows MRI images of different settings.

3.2 U-Net Architecture:

U-Net developed by Ronneberger et al. [18] is an architecture for semantic segmentation which uses a Fully Convolution Network Model. The purpose of semantic image segmentation is to give each and every pixel in a picture a class that symbolizes something. This task is usually known as a dense prediction because we're predicting each

pixel in the image [25]. U-Net is popularly used in medical image segmentation. Radiologists' analysis can be supplemented by machines using U-Net, considerably lowering the time it takes to run diagnostic procedures.

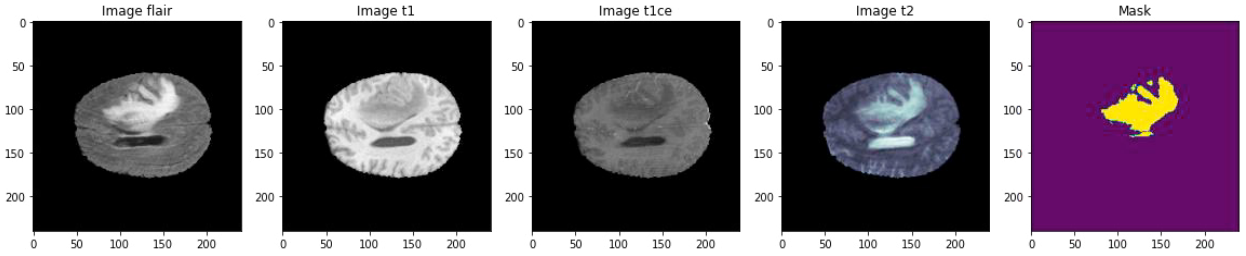

Figure 3: Visual representation of an MRI image provided in dataset

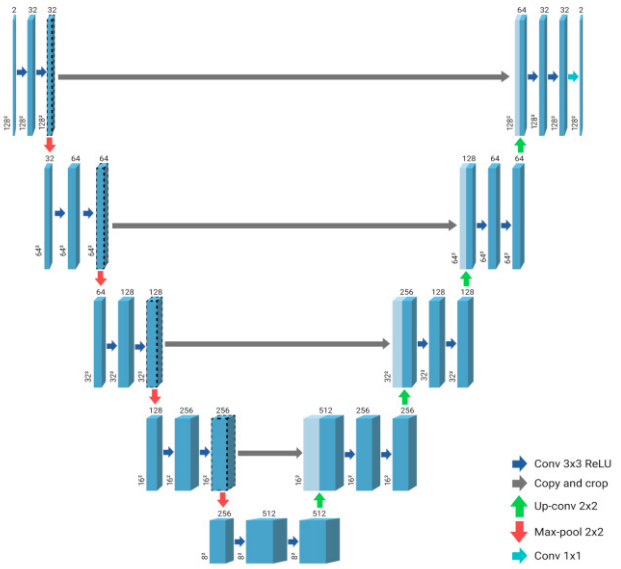

Figure 4: U-net architecture for the 3D image segmentation model.

The contracting path and the expanding path together make up the model. The reducing/contracting path follows the typical architecture of a convolutional network which downsamples an image. It is made up of two 3×3 convolutions that are applied repeatedly (unpadded convolutions), with a rectified linear unit (ReLU) [19] coming after each for down-sampling, a 2×2 max pooling operation with stride 2 is used. Each stage in the downsampling process doubles the number of feature channels. In each stage of the expansive path, the feature map is up-sampled, followed by a 2x2 convolution ("up-convolution") that cuts the number of feature channels in half, a concatenation with the proportionally cropped feature map from the contracting path, and a ReLU following each of the two 3x3 convolutions. Cropping is essential since every convolution results in the loss of border pixels. The last layer uses an 1x1 convolution to divide each 64-component feature vector into the relevant number of classes. The given network contains an aggregate of 23 convolutional layers. In the final layer, Softmax has been used as activation. Given in figure 4 is the U-net model architecture that was used in this paper.

As a loss function, the categorical cross-entropy was used here [37] given in Eq. (1) as the loss function which is popularly used in multi-class classification tasks.

$$Loss = -\sum_{i=1}^{n} l_i log(p_i), \quad (1)$$

where p_i is the probability of Softmax for the i[th] class, l_i is the truth label and n stands for the number of classes. The most commonly used metrics in semantic segmentation is the Intersection-Over-Union (IoU), or the Jaccard Index given in Eq. (2).

$$Mean\ IOU = \frac{TP}{FN+FP+TP} \quad (2)$$

To calculate the mean IoU, the overlapped area between the predicted segmentation and the ground truth is divided by the area of union between the predicted segmentation and the ground truth[38]. The dice coefficient was also used here [26] given in Eq. (3) to evaluate it as a performance metric.

$$Dice\ Coefficient = \frac{2*TP}{FN+FP+(2*TP)}, \quad (3)$$

where TP is a true positive, FP is false positive and FN is a false negative, Dice loss accounts for both local and global loss data. The Dice coefficient and the Mean IoU are quite similar. Since they are positively connected, if one asserts that model A is superior to model B at segmenting images, the other will concur. They, like the IoU, range from 0 to 1, with 1 denoting the most similarity between expected and true values.

Algorithm: Proposed UNet Model

Step 1: Normalising and resizing the BraTS dataset images.
Step 2: This is the encoder part, we use standard convolutions and a max-pooling unit (2×2) in each level, and the depth of the image slowly increases while the image size gradually reduces, starting from 128×128×2 to 8×8×512.

I. CONV2D 1: output: 128 × 128 × 32, kernel size: 3 × 3, activation function: 'ReLU';
II. MAX_POOLING2D: output: 64 × 64 × 32, pool size: 2 × 2;
III. CONV2D 2: output: 64 × 64 × 64, kernel size: 3 × 3, activation function: 'ReLU';
IV. CONV2D 3: output: 64 × 64 × 64, kernel size: 3 × 3, activation function: 'ReLU';
V. MAX_POOLING2D: output: 32 × 32 × 64, pool size: 2 × 2;
VI. CONV2D 4: output: 32 × 32 × 128, kernel size: 3 × 3, activation function: 'ReLU';
VII. CONV2D 5: output: 32 × 32 × 128, kernel size: 3 × 3, activation function: 'ReLU';
VIII. MAX_POOLING2D: output: 16 × 16 × 128, pool size: 2 × 2;
IX. CONV2D 6: output: 16 × 16 × 256, kernel size: 3 × 3, activation function: 'ReLU';
X. CONV2D 7: output: 32 × 32 × 256, kernel size: 3 × 3, activation function: 'ReLU';
XI. MAX_POOLING2D: output: 8 × 8 × 256, pool size: 2 × 2;
XII. CONV2D 8: output: 8 × 8 × 512, kernel size: 3 × 3, activation function: 'ReLU';
XIII. CONV2D 9: output: 8 × 8 × 512, kernel size: 3 × 3, activation function: 'ReLU';

Step 3: Then, in the decoder, we used transposed convolutions along with standard convolutions to gradually expand the image size while reducing the depth, from 8×8×512 to 128×128×2.

I. DROPOUT
II. UP_SAMPLING_2D: output: 16 × 16 × 512, kernel size: 2 × 2, activation function: 'ReLU';
III. CONV2D 10: output: 16 × 16 × 256, kernel size: 3 × 3, activation function: 'ReLU';
IV. CONCATENATE 1: output: 16 × 16 × 512;
V. CONV2D 11: output: 16 × 16 × 256, kernel size: 3 × 3, activation function: 'ReLU';
VI. CONV2D 12: output: 16 × 16 × 256, kernel size: 3 × 3, activation function: 'ReLU';
VII. UP_SAMPLING_2D: output: 32 × 32 × 256, kernel size: 2 × 2, activation function: 'ReLU';
VIII. CONV2D 13: output: 32× 32× 128, kernel size: 3 × 3, activation function: 'ReLU';
IX. CONCATENATE 2: output: 32 × 32 × 256;
X. CONV2D 14: output: 32× 32× 128, kernel size: 3 × 3, activation function: 'ReLU';
XI. CONV2D 15: output: 32× 32× 128, kernel size: 3 × 3, activation function: 'ReLU';
XII. UP_SAMPLING_2D: output: 64 × 64 × 128, kernel size: 2 × 2, activation function: 'ReLU';
XIII. CONV2D 16: output: 64 × 64 × 128, kernel size: 3 × 3, activation function: 'ReLU';

XIV. CONCATENATE 3: output: 64 × 64 × 128;
XV. CONV2D 17: output: 64 × 64 × 64, kernel size: 3 × 3, activation function: 'ReLU';
XVI. CONV2D 18: output: 64 × 64 × 64, kernel size: 3 × 3, activation function: 'ReLU';
XVII. UP_SAMPLING_2D: output: 128 × 128 × 64, kernel size: 2 × 2, activation function: 'ReLU';
XVIII. CONV2D 19: output: 128 × 128 × 32, kernel size: 3 × 3, activation function: 'ReLU';
XIX. CONCATENATE 4: output: 128× 128× 64;
XX. CONV2D 20: output: 128 × 128 × 32, kernel size: 3 × 3, activation function: 'ReLU';
XXI. CONV2D 19: output: 128 × 128 × 32, kernel size: 3 × 3, activation function: 'ReLU';
XXII. CONV2D 19: output: 128 × 128 × 4, kernel size: 3 × 3, activation function: 'Softmax';

Step 4: The encoder part's layers are skip connected and are concatenated with the decoder part's layers (those are mentioned as gray lines in the above diagram), due to which the U-Nets to generate an image in the decoder part using fine-grained details learned in the encoder part.
Step 5: Finally, the loss function and model were set up. Our optimizer is Adam, and the loss function used here is Categorical Cross-Entropy Loss.

4. Results:

The dataset used here was MICCAI BRATS 2020 Dataset contains 371 training files which was taken from Kaggle. The model was trained on Kaggle with the specifications 2-core of Intel Xeon as CPU, Tesla P100 16GB VRAM as GPU, with 13GB RAM. In the training process, 35 epochs were run to train this model which took us about 14 hours to train.

The challenge of identifying a tumor is quite difficult. The position, form, and structure of tumors differ greatly from one patient to the next, making segmentation a difficult process. In figure 5, various scans of the same brain sliced segment from different patients, clearly indicate the tumor diversity. The position of the tumor is obviously different in each of the eight images/patients presented. In reality, Figure 5 shows the tumor can be divided into many regions [28].

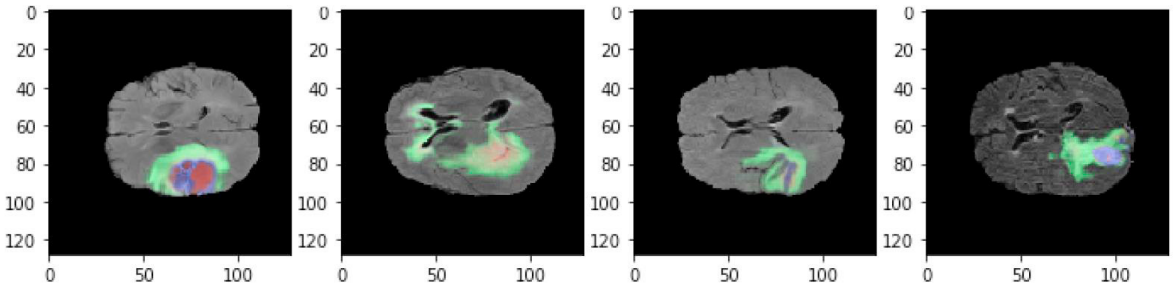

Figure 5: Regions in which brain tumor is located for four different patients

5.1 Dataset Description

In order to perform the task, we would need a dataset with a lot of MRI images, so for this paper, we are going to take the BRATS2020 Dataset. The multimodal scans of the BraTS dataset are available as NIfTI files (.nii.gz) - a commonly used medical imaging format to store brain imaging data obtained using MRI and describe different MRI settings .T1-weighted, native image, sagittal or axial 2D acquisitions, with 1–6 mm slice thickness [13].

T1c: T1-weighted, contrast-enhanced (Gadolinium) image, with 3D acquisition and 1 mm isotropic voxel size for most patients. T2-weighted image, axial 2D acquisition, with 2–6 mm slice thickness. T2-weighted FLAIR image, axial, coronal, or sagittal 2D acquisitions, 2–6 mm slice thickness [21].

Data were acquired with different clinical protocols and various scanners from multiple (n=19) institutions. All of the imaging datasets were manually segmented by one to four raters using the same annotation technique, and their annotations were reviewed and validated by professional neuro-radiologists. Annotations include the peritumoral

edema (ED - label 2), the GD-enhancing tumor (ET - label 4), and the necrotic and non-enhancing tumor core (NCR/NET — label 1), as described both in the BraTS 2012-2013 TMI paper and in the latest BraTS summarizing the paper. After pre-processing, the data are disseminated, which includes being co-registered to the identical anatomical template, interpolated to original resolution (1 mm^3), and skull-stripped [36].

5.2 Training

Initially the model was trained with 15 epochs, but the nature of the graphs showed gradual improvement, then in order to get better results the number of epochs was increased to 25 where the results were better but in order to reinforce our results further it was increased to 35 epochs where the results were getting stabilized. Finally, the model was trained with 35 epochs and it took 12 hours for the training process to be complete so that it be used further the model was saved in an h5 file named "model_x1_1.h5".

While training the model, we stored all the metrics for each epoch. Then the saved model was loaded and used to plot metrics for training and validation. In Figure 8, the graphs show the training metrics where the blue line symbolizes the training metric and the red line describes the validation metric, where the y-axis indicates the number of epochs and the x-axis indicates the score. Figure 6(a) shows the accuracy of training and validation with varying epochs. It states that training accuracy is slightly higher than validation accuracy and they reach the plateau at about 20 epochs. Figure 6(b) shows training and validation loss, and the difference is about 0.01 so it can be concluded that it is a good fit. Figure 6(c) shows a significant increase in dice with a subsequent increase in the number of epochs in both training and validation. Finally, figure 6(d) shows the Mean IoU of the training and validation set. The mean IoU score of training and validation reached a value greater than 0.5 after about 15 epochs, and greater than 0.8 after about 25 epochs which is a good score to have.

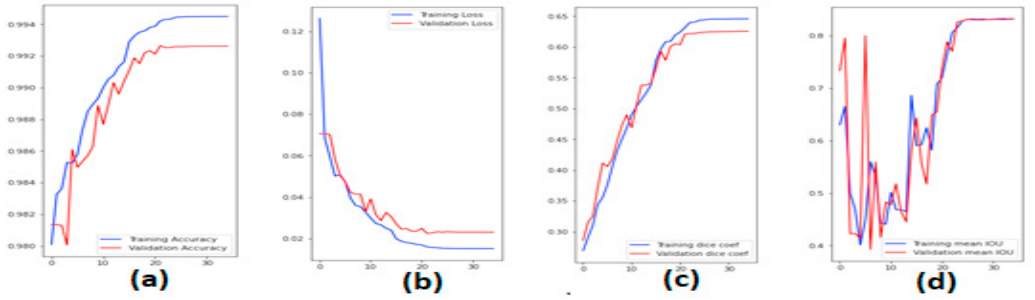

Figure 6: (a) Graph describing the accuracy, (b) loss for each epoch, (c) Graph describing the Dice Coefficient, and (d) and Mean IOU for each epoch

5.3 Predictions

For predicting the presence of tumor in the brain and classifying its classes the model was trained and used, then the original MRI image along with the ground truth images and the prediction classes were plotted for proper visualization of the predictions. In the predictions below Random Images were taken in order to visualize how accurately the algorithm is predicting. In Figures 7, and 8, which are images of a brain containing a tumor, it can be seen our prediction corresponds accurately with the ground truth.

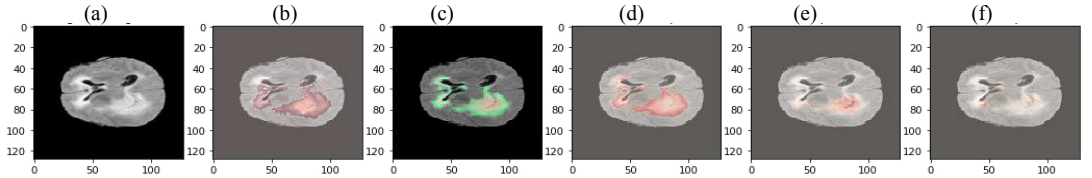

Figure 7: Prediction of Sample Data 1.

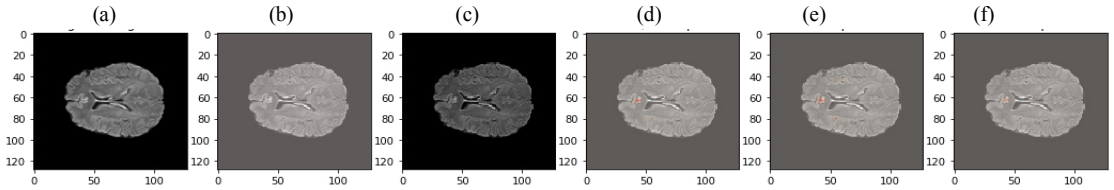

Figure 8: Prediction of Sample Data 2.

In Figure 7 to Figure 8 it is observed that the ground truth image and the predictions from left to right where (a) is the original image, (b) is the ground truth image, (c) shows all the tumor classification, (d) is the prediction for Necrotic/Core region, (e) is the prediction for Edema region and finally (f) is the Enhancing region.

5.4 Evaluation Metrics

The model was evaluated to generate different metrics using the test data by using a data generator to randomize the data, and the batch size taken was 100. The following metrics were obtained that are represented in table 1 given below, accuracy [39], loss, dice coefficient [26], mean IOU [38], precision [39], sensitivity [40], and specificity [41]. The saved model was used to evaluate the given metrics to create a scorecard where these metrics are shown for both training set and validation set.

Table 1: Metric scores for training and validation of U-net model

Metric	**Training Score**	**Validation Score**
Accuracy	99.46	99.39
Loss	01.49	01.71
Dice Coefficient	67.03	65.67
Mean IOU	80.23	83.26
Precision	99.48	99.41
Sensitivity	99.32	99.27
Specificity	99.82	99.80

5.5 Comparative Analysis

In order to represent how much improvement U-Net Architecture provides compared to some other popular methods of brain tumor detection can be clearly seen by doing a comparative study, where we take the same dataset and find out the metrics for other algorithms. Table 2 below shows a tabular representation of the comparative analysis.

Table 2: Comparative analysis of U-Net, ResNet 50, and VGG16

Metric	**VGG16**	**ResNet50**	**U-Net**
Accuracy	98.69	97.18	99.39
Loss	04.33	09.85	01.71
Dice Coefficient	34.56	34.02	65.67
Mean IOU	68.17	37.56	83.26
Precision	99.22	98.14	99.41
Sensitivity	98.17	96.78	99.27
Specificity	99.73	99.39	99.80

As it is observed, U-Net outperformed ResNet and VGG-16 (popular CNN architectures in the image processing domain) in every metric. U-Net is highly beneficial and accurate for medical image processing. Although a typical convolutional neural network emphasizes image classifications, getting a single label as output and using an image as input, biological images require us to not only detect whether there is a sickness but also to find the anomalous location.

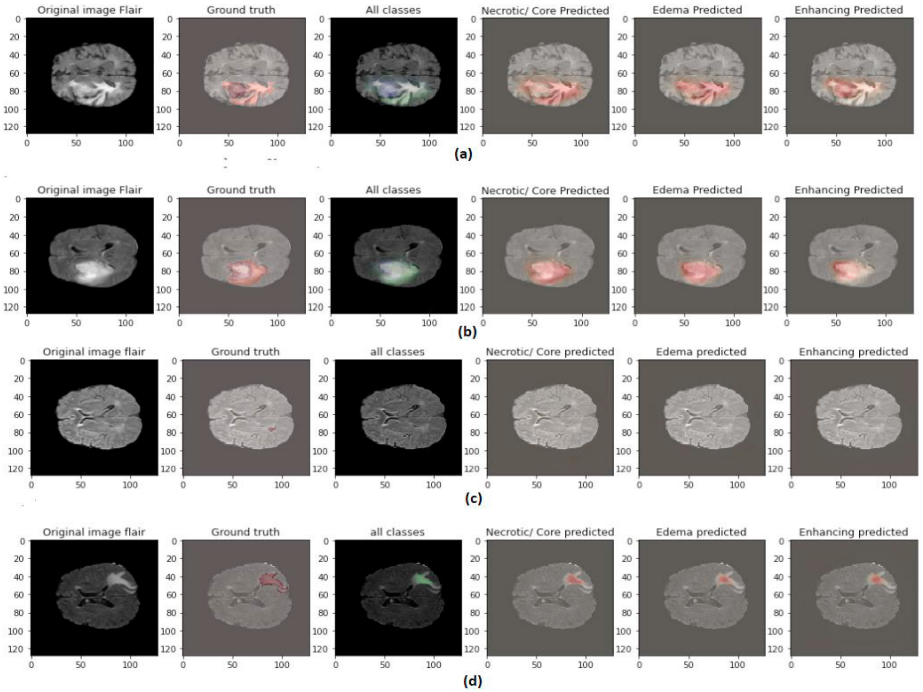

Figure 9: Prediction using existing models: (a) VGG-16, (b) VGG-19, (c) ResNet-50, and (d) ResNet-34.

Figure 9 shows the resultant images from four existing methods viz. VGG-16, VGG-19, ResNet-50, and ResNet-34. In the subjective evaluation, VGG-16 produced better result than other existing models. Figure 9 exhibits visually clear images with detected abnormalities in comparison with four baseline models.

Though U-Net outperformed the other algorithms, it also comes with a couple of drawbacks. Working with 3D images requires a lot of computational power and the images require a lot of storage space, so high-powered GPU and high-capacity storage are required. Finally, since U-net has a lot of layers, the training process takes a significant amount of time, so making tweaks may result in loss of time.

6. Conclusion

The primary goal of this research focuses on development of automated medical imaging segmentation i.e. quick detection of tumors in the brain. In medical imaging assistive segmentation by radiologists prove to be very time-consuming and resource intensive which might not be available in remote regions. So, this task of advanced automation techniques for brain tumor detection can be proved to be very beneficial in a substantial amount of cases. In order to overcome this obstacle, the primary algorithm used in this paper was U-Net, which helped in outlining the tumor and it was very close to the ground truth and it also gave highly accurate predictions in MRI images. Different methods of progressive and innovative brain tumor detection approaches are discussed in this article. The initial preprocessed segment uses median filtering techniques for preprocessing MRI images, and we have achieved a validation accuracy of 99 % performed on the BRATS2020 Dataset. As a result, the target area is segmented, and the presence of the tumor may be determined using the approach provided here, allowing clinicians to plan therapy and monitor tumors during the diagnosis period. The advantages of this approach are that it enhances the level of image

segmentation and its spatial localization, and hence it performs better in comparison to other systems. It is faster to train and requires less time to calculate than different networks with less number of parameters.

Further studies will include enhancing accuracy with a low rate of error by employing various classifier algorithms. Further, this can be modified to be used to predict the survivability of patients having brain tumors. Future work may include using larger and varied datasets which will help to test in real-life scenarios and clinical trials.

References

[1] Ahuja S, Panigrahi BK, Gandhi T (2020). "Transfer Learning Based Brain Tumour Detection and Segmentation using Superpixel Technique," 2020 International Conference on Contemporary Computing and Applications (IC3A), 2020, pp. 244-249

[2] Tripathi P, Singh VK, Trivedi MC (2021). "Brain tumor segmentation in magnetic resonance imaging using OKM approach", Materials Today: Proceedings, Volume 37, Pages 1334-1340.

[3] Miglani A, Madan H, Kumar S, Kumar S (2021). "A Literature Review on Brain Tumour Detection and Segmentation," 2021 5th International Conference on Intelligent Computing and Control Systems (ICICCS), pp. 1513-1519

[4] Cherguif H, Riffi J, Mahraz,M A, Yahyaouy A, Tairi A (2019). "Brain Tumour Segmentation Based on Deep Learning," 2019 International Conference on Intelligent Systems and Advanced Computing Sciences (ISACS), pp. 1-8

[5] Mesut T, Zafer C, Burhan E, (2020). "Classification of Brain MRI Using Hyper Column Technique with Convolutional Neural Network and Feature Selection Method". Expert Systems with Applications. 149.

[6] Choudhury CL, Mahanty C, Kumar R, Mishra BK, (2020). "Brain Tumour Detection and Classification Using Convolutional Neural Network and Deep Neural Network," 2020 International Conference on Computer Science, Engineering and Applications (ICCSEA), pp. 1-4

[7] Thias AH, Al Mubarok AF, Handayani A, Danudirdjo D, Rajab TE, (2019). "Brain Tumor Semi-automatic Segmentation on MRI T1-weighted Images using Active Contour Models," 2019 International Conference on Mechatronics, Robotics and Systems Engineering (MoRSE), pp. 217-221

[8] Çinar A, Yildirim M, (2020). "Detection of tumors on brain MRI images using the hybrid convolutional neural network architecture", Med. Hypotheses, vol. 139, p. 109684

[9] Abdelaziz Ismael SA, Mohammed A, Hefny H (2020). "An enhanced deep learning approach for brain cancer MRI images classification using residual networks". Artif Intell Med.

[10] Badža MM., Marko CB (2020). "Classification of Brain Tumors from MRI Images Using a Convolutional Neural Network" Applied Sciences 10,

[11] Afshar P, Mohammadi A, Plataniotis KN, (2020). "BayesCap: A Bayesian Approach to Brain Tumour Classification Using Capsule Networks," in IEEE Signal Processing Letters, vol. 27, pp. 2024-2028.

[12] Noreen N, Palaniappam S, Qayyum A, Ahmad I, Imran M, (2020) "Attention-Guided Version of 2D UNet for Automatic Brain Tumor Segmentation," IEEE Access, Volume: 8.

[13] https://www.kaggle.com/navoneel/brain-mri-images-for-brain-tumor-detection/metadata

[14] Özyurt F, Sert E, Avcı D, (2020). "An expert system for brain tumour detection: Fuzzy C-means with super resolution and convolutional neural network with extreme learning machine", Med. Hypotheses, vol. 134, p. 109433.

[15] Lei X, Yu X, Chi J, Wang Y, Zhang J, Wu C, (2020). "Brain tumour segmentation in MR images using a sparse constrained level set algorithm", in Expert Systems With Applications, Elsevier.

[16] Leena B, Jayanthi A, (2020). "Brain tumour segmentation and classification via adaptive CLFAHE with hybrid classification ," in Int J Imaging Syst Technol. Wiley.

[17] Bansal N, Dawande P, Shukla S, Acharya S (2020). "Effect of lifestyle and dietary factors in the development of brain tumors". J Family Med Prim Care. 30;9(10):5200-5204

[18] Ronneberger, O., Fischer, P., Brox, T (2015). "U-Net: Convolutional Networks for Biomedical Image Segmentation". In: Medical Image Computing and Computer-Assisted Intervention. pp. 234–241 (2015).

[19] Abien Fred A (2018). "Deep Learning using Rectified Linear Units (ReLU)." ArXiv abs/1803.08375

[20] Ghosh SK, Biswas B, Ghosh A (2020). "Restoration of Mammograms by Using Deep Convolutional Denoising Auto-Encoders". In: Behera, H., Nayak, J., Naik, B., Pelusi, D. (eds) Computational Intelligence in Data Mining. Advances in Intelligent Systems and Computing, vol 990. Springer, Singapore. https://doi.org/10.1007/978-981-13-8676-3_38

[21] https://www.med.upenn.edu/cbica/brats2020/data.html

[22] Menze BH, Jakab A, Bauer S, Kalpathy-Cramer J, Farahani K, Kirby J, et al. (2015). "The Multimodal Brain Tumor Image Segmentation Benchmark (BRATS)", IEEE Transactions on Medical Imaging 34(10), 1993-2024 DOI: 10.1109/TMI.2014.2377694

[23] Bakas S, Akbari H, Sotiras A, Bilello M, Rozycki M, et al. (2017). "Advancing The Cancer Genome Atlas glioma MRI collections with expert segmentation labels and radiomic features", Nature Scientific Data, 4:170117.

[24] Bakas S, Reyes M, Jakab A, Bauer S, Rempfler M, Crimi A, et al. (2018). "Identifying the Best Machine Learning Algorithms for Brain Tumor Segmentation, Progression Assessment, and Overall Survival Prediction in the BRATS Challenge", arXiv preprint arXiv:1811.02629 (2018).
[25] Long J, Shelhamer E, Darrell T (2015). "Fully convolutional networks for semantic segmentation," 2015 IEEE Conference on Computer Vision and Pattern Recognition (CVPR), pp. 3431-3440
[26] Ghosh SK, Mitra A, Ghosh A (2020). "A novel intuitionistic fuzzy soft set entrenched mammogram segmentation under Multigranulation approximation for breast cancer detection in early stages". Expert Systems with Applications (2020).
[27] Kenneth A, et al.(2019). "Challenges to curing primary brain tumours." Nature reviews. Clinical oncology vol. 16,8 (2019): 509-520.
[28] Rahimpour M, Goffin K, Koole M (2019). "Convolutional Neural Networks for Brain Tumor Segmentation Using Different Sets of MRI Sequences," 2019 IEEE Nuclear Science Symposium and Medical Imaging Conference (NSS/MIC), pp. 1-3.
[29] Zeljkovic V, et al. (2014). "Automatic brain tumor detection and segmentation in MR images," 2014 Pan American Health Care Exchanges (PAHCE).
[30] Kumar S, Negi S, Singh JN, Gaurav A (2018). "Brain Tumor Segmentation and Classification Using MRI Images via Fully Convolution Neural Networks," 2018 International Conference on Advances in Computing, Communication Control and Networking (ICACCCN), pp. 1178-1181.
[31] Krupinski, EA, Jiang Y (2008). "Anniversary Paper: Evaluation of medical imaging systems". Med. Phys., 35: 645-659.
[32] Adrienne E, Campbell W, Ramasawmy R, Restivo MC, Bhattacharya I, Basar B et al. (2019). "Opportunities in Interventional and Diagnostic Imaging by Using High-Performance Low-Field-Strength MRI" Radiology. 293:2, 384-393.
[33] Zhou SK, et al. (2021). "A Review of Deep Learning in Medical Imaging: Imaging Traits, Technology Trends, Case Studies With Progress Highlights, and Future Promises," in Proceedings of the IEEE, vol. 109, no. 5, pp. 820-838.
[34] Robba C, Goffi A, Geeraerts T, et al. (2019). "Brain ultrasonography: methodology, basic and advanced principles and clinical applications". A narrative review. Intensive Care Med 45, 913–927.
[35] Zhou SK, et al. (2021). "A Review of Deep Learning in Medical Imaging: Imaging Traits, Technology Trends, Case Studies With Progress Highlights, and Future Promises," in Proceedings of the IEEE, vol. 109, no. 5, pp. 820-838.
[36] Bhushan C, Haldar JP, Choi S, Joshi AA, Shattuck DW, Leahy RM (2015). "Co-registration and distortion correction of diffusion and anatomical images based on inverse contrast normalization". Neuroimage. 115 pp:269-280.
[37] Yeung M, Sala E, Schönlieb CB, Rundo L (2022). "Unified Focal loss: Generalising Dice and cross entropy-based losses to handle class imbalanced medical image segmentation", Computerized Medical Imaging and Graphics, Volume 95.
[38] Amirreza S, Bansal S, Zhen L, Irfan E, Byron B. (2017). "One-Shot Learning for Semantic Segmentation". arXiv preprint arXiv:1709.03410.
[39] Rizwan I, Haque I, Neubert J (2020). "Deep learning approaches to biomedical image segmentation", Informatics in Medicine Unlocked, Volume 18.
[40] Rezaie A, Achanta R, Godio M, Beyer K (2020). "Comparison of crack segmentation using digital image correlation measurements and deep learning", Construction and Building Materials, Volume 261.
[41] Lima R, Pozo A, Mendiburu A, Santana R (2021). "Automatic Design of Deep Neural Networks Applied to Image Segmentation Problems". In: Hu, T., Lourenço, N., Medvet, E. (eds) Genetic Programming. EuroGP. Lecture Notes in Computer Science(), vol 12691. Springer.
[42] Rehman A, Khan MA, Saba T, Mehmood Z, Tariq U, Ayesha N (2021). "Microscopic brain tumor detection and classification using 3D CNN and feature selection architecture". Microsc Res Tech. 84: 133– 149.